Journal of Innovative Optical Health Sciences
Vol. 2, No. 2 (2009) 201–208

World Scientific
www.worldscientific.com

INTRINSIC OPTICAL SIGNAL IMAGING OF RETINAL ACTIVITY IN FROG EYE

XIN-CHENG YAO*,‡, LEI LIU† and YANG-GUO LI*
*Department of Biomedical Engineering
University of Alabama at Birmingham
Birmingham, AL 35294, USA
†Department of Optometry
University of Alabama at Birmingham
Birmingham, AL 35294, USA
‡xcy@uab.edu

Using a near-infrared (NIR) light flood-illumination imager equipped with a high-speed (120 Hz) CCD camera, we demonstrated optical imaging of stimulus-evoked retinal activity in isolated, but intact, frog eye. Both fast and slow transient intrinsic optical signals (IOSs) were observed. Fast optical response occurred immediately after the stimulus onset, could reach peak magnitude within 100 ms, and correlated tightly with ON and OFF edges of the visible light stimulus; while slow optical response lasted a relatively long time (many seconds). High-resolution images revealed both positive (increasing) and negative (decreasing) IOSs, and dynamic optical change at individual CCD pixels could often exceed 10% of the background light intensity. Our experiment on isolated eye suggests that further development of fast, high (sub-cellular) resolution fundus imager will allow robust detection of fast IOSs *in vivo*, and thus allow noninvasive, three-dimensional evaluation of retinal neural function.

Keywords: Near-infrared light imaging; neural activity; retina; visual information processing; retinal diagnosis.

1. Introduction

Eye diseases, such as age-related macular degeneration (AMD),[1] glaucoma,[2,3] diabetic retinopathy (DR),[4,5] are known to cause pathological changes of photoreceptors and/or inner retinal neurons, which ultimately lead to vision losses and even complete blindness. Early detection is an important step toward preventing vision loss associated with these diseases. Because of the delicate, complex structure of the retina,[6] high-resolution functional imaging is desirable for improved retinal diagnosis and treatment evaluation. Conventional morphological assessment of the retina, such as fundus examination, does not see retinal neural cells directly, because they are almost transparent. Abnormal fundus findings are therefore not always correlated with functional changes.[1,7,8] Conventional electroretinogram (ERG)[9] and multifocal ERG[10,11] are frequently used to measure retinal neural activities, but the relationship between ERG and retinal neural cells is not direct. Because ERG signal is pooled from an extended retinal area, the effect of localized dysfunction is likely to be masked.

Transient intrinsic optical signals (IOSs) have been recorded for spatiotemporal mapping of stimulus-evoked neural activities in the brain cortex.[12–16] Recently, several imaging techniques, such as near-infrared (NIR) light flood-illumination microscope,[17] fundus camera,[18–20] adaptive optics imager,[21,22] and functional optical coherence tomography[23–25] have been used for IOS imaging of

isolated retinas,[17,23,25–28] anesthetized animals,[19,24] and humans.[18,21,22] IOS imaging holds promise for noninvasive, high-resolution evaluation of retinal neural function. However, practical application of the IOS imaging still has to overcome inconsistency in IOS time course and signal polarity. Both fast and slow IOSs have been observed during light stimulation of the retina. In general, stimulus-evoked neural activities, metabolic changes, and activities of other ocular tissues all can produce IOSs. Slow IOSs, which may last many seconds after light stimulation, are mainly associated with stimulus-evoked metabolic changes. They reflect one aspect of retinal response to light stimulation, but their relation to actual neural activity is indirect. Fast IOSs, which have time courses comparable to electrophysiological kinetics of the neural activities, hold promise for direct functional evaluation of the photoreceptors and inner neurons. *In vivo* recording of transient IOSs in photoreceptors has been obtained with functional OCT[24] and adaptive optics[19,21] imaging systems, but *in vivo* imaging of fast IOSs, which have time courses comparable to ERG kinetics, such as retinal ON and OFF responses, has not been reported.

Isolated retina is a simple preparation for understanding of the sources and biophysical mechanisms of fast IOSs and for optimization of the instrument design. We have been successful in imaging fast IOSs in isolated amphibian retinas, which have time courses comparable to ERG kinetics.[17,26–28] IOSs in single pixels of high-resolution ($\sim\mu$m) imaging often exceed 5% $\Delta I/I$, allowing robust IOS imaging with single pass measurements.[17] Dark-field and polarization imaging further improves the sensitivity to detect fast IOSs.[28] Using a step-visible light stimulus to activate the retina, we have shown that fast IOSs were tightly correlated with electrophysiological ON and OFF responses. Our experiments with isolated retinas indicated that both positive and negative IOSs could occur in retinal areas adjacent to light stimulation site, which suggested that high spatial resolution that minimized spatial pooling is critical for high-performance IOS imaging.

Our long-term goal is to develop high-spatiotemporal-resolution IOS imaging technology that allows direct *in vivo* mapping of retinal neural activities. Without complicated blood changes and eye movements, isolated eye, free from the complication of hemodynamic changes and eye movements, can be used as a transitional preparation between isolated retina and *in vivo* eye. In this study, we demonstrate the feasibility of IOS imaging of retinal ON and OFF responses in isolated, but intact, frog eye.

2. Materials and Methods

2.1. *Preparation of isolated eye*

We used isolated frog (*Rana pipiens*) eyes for recording IOS imaging of fast retinal neural activity through intact ocular optics. The experiments were performed following protocols approved by the Institutional Animal Care and Use Committee of University of Alabama at Birmingham. The frog was dark-adapted for 20–30 min before rapid euthanasia by decapitation and removal of the eyes. The procedure was conducted in a dark room with dim red illumination. The isolated frog eye was transferred into a recording chamber filled with Ringer's solution containing (in mM): 110 NaCl, 2.5 KCl, 1.6 MgCl2, 1.0 CaCl2, 22 NaHCO3, and 10 D-glucose.[29]

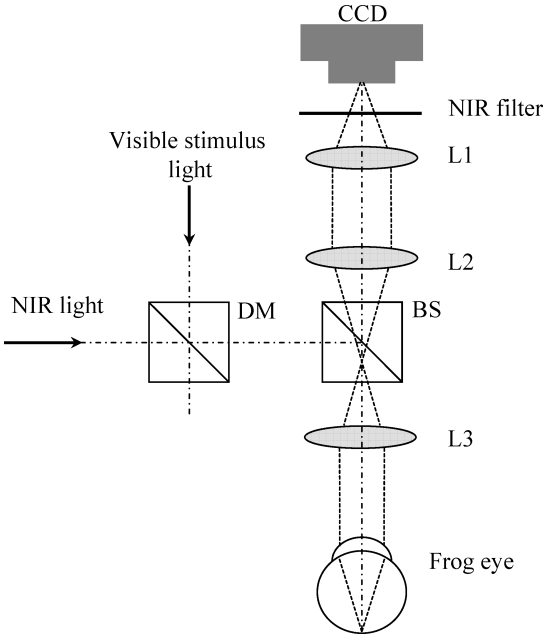

Fig. 1. Schematic diagram of the flood-illumination imager for IOS imaging of intact frog eye. During the measurement, the retina was illuminated continuously by the NIR light for recording of stimulus-evoked IOSs. The visible stimulus light was used to activate the retina. At the dichroic mirror (DM), visible stimulus light was reflected and NIR recording light was passed through. BS was a 50/50 beam splitter. The NIR filter was used to block reflected visible stimulus light, and allow the NIR probe light to reach the CCD camera.

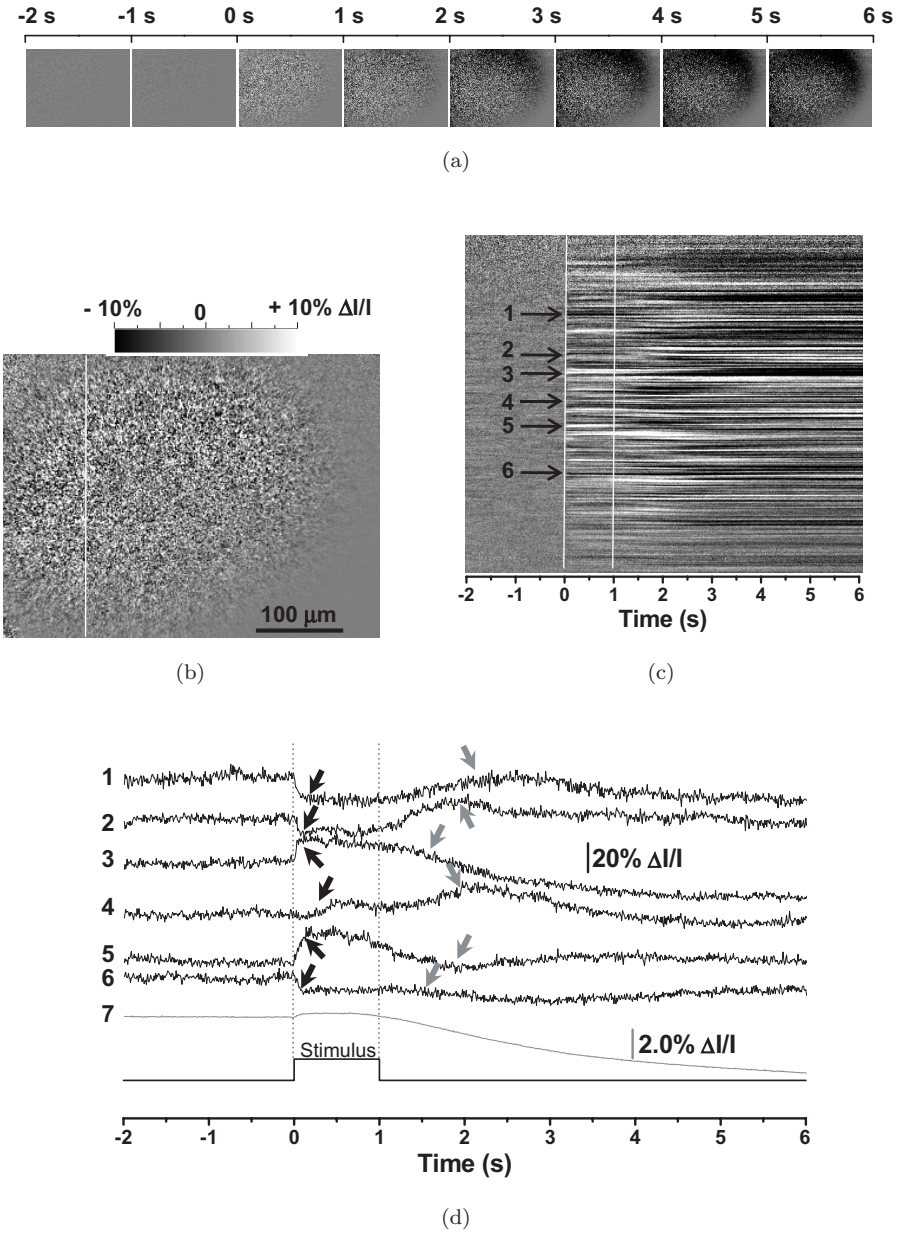

Fig. 2. High-resolution IOS imaging of retinal neural activity in isolated eye with intact ocular optics. Raw frames were acquired with a frame speed of 120 frames/s. (a) IOS image sequence shows dynamic optical responses of the retina. Each illustrated frame is an average of 120 frames over one second interval. The visible light stimulus was delivered at time 0, and lasted for 1 s. (b) Enlarged picture of the third frame in (a). (c) M-sequence of the retinal area indicated by the white line in (b). (d) Temporal changes of IOSs of representative pixels. Black tracings 1–6 correspond to the areas pointed by arrowheads 1–6 in (c). Gray tracing 7 is the averaged signal of the image area. Note that large IOSs of single pixels (tracings 1–6) can be $>10\%$.

2.2. *Experimental setup*

A NIR light flood-illumination imager was constructed for IOS imaging of isolated frog eye (Fig. 1). During the recording, intact frog eye was immersed in the recording chamber filled with Ringer's solution. The recording chamber was placed into a customer-designed holder, which allowed easy adjustment of the optical axis of frog eye relative to NIR illumination light. While the retina was illuminated continuously with a NIR light (785 nm) for recording of IOSs, a white light flash (1 s) was used to activate the retina. A fast CCD camera was used to record IOSs. The optical images presented in this article were recorded with a speed of 120 frames/s, and each frame consisted of 640×480 pixels. The optical magnification, M, of

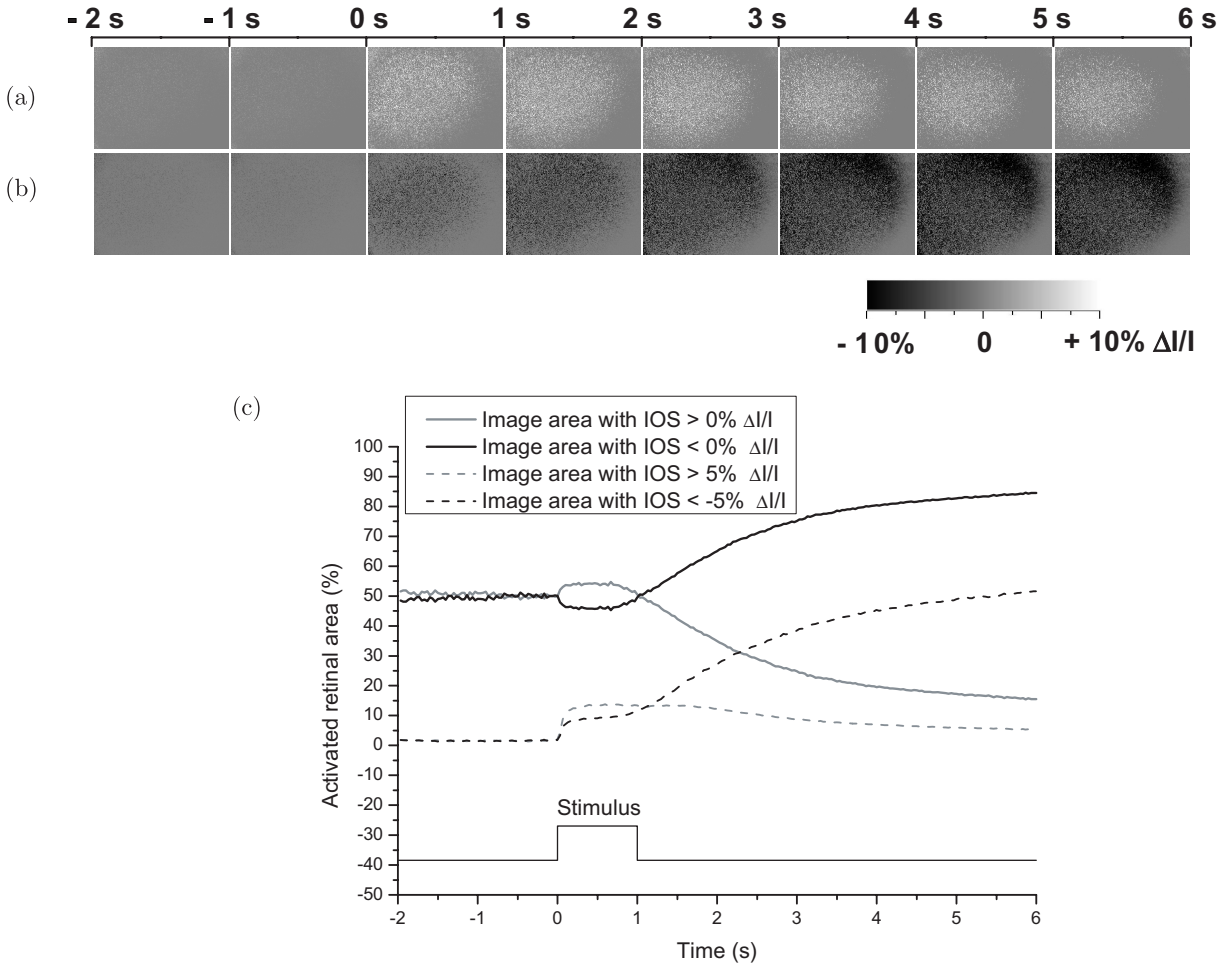

Fig. 3. Positive and negative IOSs. (a) Dynamic optical patterns of positive IOSs. (b) Dynamic optical patterns of negative IOSs. (c) Statistics of image area with positive and negative IOSs.

the imaging system shown in Fig. 1 can be calculated as follows:

$$M = (f_1 \times f_3)/(f_2 \times f_{eye}), \qquad (1)$$

where f_1 (50 mm), f_2 (60 mm), f_3 (40 mm), and f_{eye} are the focal lengths of the lens L1, L2, L3, and frog eye, respectively. We assume that $f_{eye} = 2.87$ mm,[30] and thus $M \approx 11.6$. In theory, each CCD pixel ($7.4\,\mu$m $\times$ $7.4\,\mu$m) corresponded to a $0.64\,\mu$m $\times$ $0.64\,\mu$m area at the frog retina, although practical imaging resolution can be reduced due to optical aberrations of the lenses and frog ocular optics.

2.3. *IOS imaging and data processing*

The IOS images (Fig. 2(a)) shown in this article represented stimulus-evoked optical responses in the unit of $\Delta I/I$, where ΔI was the dynamic optical changes and I was the background light intensity. The IOS images were constructed as follows: (1) Pre-stimulus baseline images were averaged, pixel by pixel, and the averaged intensity of each pixel was taken as the background light intensity I of each pixel; (2) The background light intensity I was subtracted from each recorded frame, pixel by pixel, to get ΔI of each pixel of the image sequence; (3) Image sequence (Fig. 2(a)) of $\Delta I/I$ was constructed to show dynamic IOS patterns of the activated retina. M-sequence image (Fig. 2(c)) was used for simultaneous depiction of temporal and spatial dynamics of the IOSs along a selected line. IOSs of individual pixels (Fig. 2(d)) were used to show the time courses of transient optical responses.

In order to investigate the IOSs with opposite (i.e. positive and negative) polarities, we separated IOS patterns with positive (Fig. 3(a)) and negative (Fig. 3(b)) optical changes. The dynamic fractional ratios of the activated retinal areas with positive

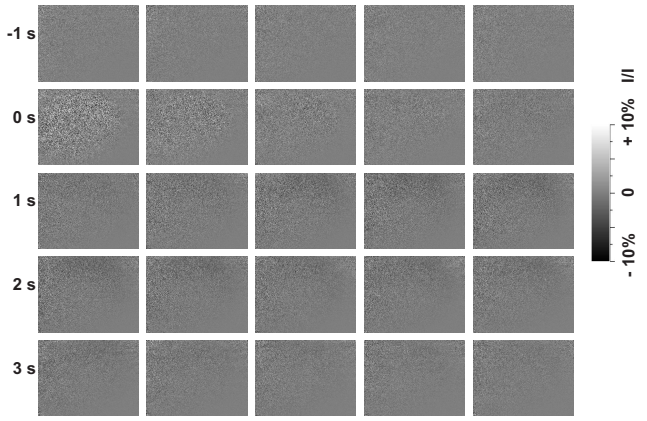

(a)

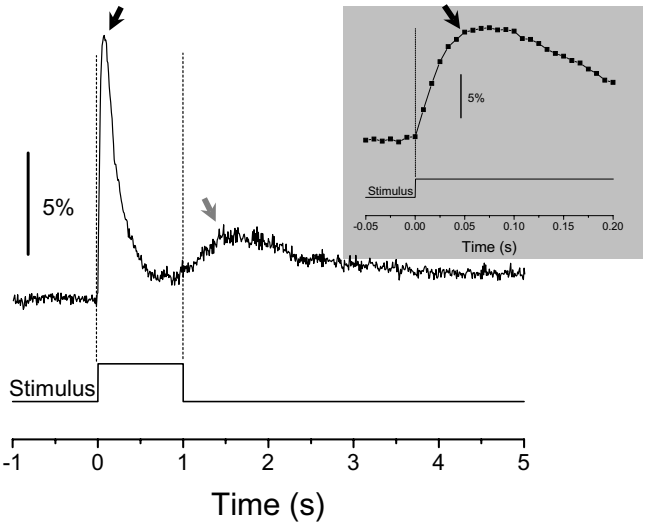

(b)

Fig. 4. (a) Differential IOSs. Raw frames were acquired with a frame speed of 120 frames/s. Each illustrated frame is an average of 24 frames over 200 ms interval. One-second (five frames) pre-stimulus baseline images are presented. (b) Statistics of activated retinal area that has optical response with magnitude $|IOS| > 2.5\%\Delta I/I$. Inset panel shows an enlarged display of the early optical response.

and negative optical signals were also quantitatively analyzed (Fig. 3(c)).

Differential IOS images (Fig. 4(a)) were used to minimize the effect of slow optical responses on the fast IOSs. The construction of differential IOS images was calculated as:

$$IOS_{t(x,y)} = (I_{t(x,y)} - I_{ref(x,y)})/I_{ref(x,y)}, \qquad (2)$$

where $I_{t(x,y)}$ is the intensity value of a pixel (x, y) at a time point t; $I_{ref(x,y)}$ is the averaged intensity value, which can be quantified by:

$$I_{ref(x,y)} = \left(\sum\nolimits_{i=t-m}^{i=t-1} I_{i(x,y)}\right)/m. \qquad (3)$$

It served as the dynamic reference baseline for the calculation of the differential IOS at pixel (x, y). In other words, the averaged pixel values of m frames recorded before the time point t is used as a reference baseline to calculate the differential IOS. Based on the differential images (Fig. 4(a)), percentage ratio of the image area with optical response $|IOS| > 2.5\%\ \Delta I/I$ was calculated to show dynamic fractional change of the activated retinal area (Fig. 4(b)). A magnitude threshold, $|IOS| > 2.5\%\ \Delta I/I$, was used to reduce the effect of dynamic background noise.

3. Experimental Results

3.1. *ON and OFF responses in frog eye*

Using the optical imager shown in Fig. 1, robust IOSs were observed from single pass measurements. Figure 2 represents transient IOSs recorded from the frog eye activated by a visible light stimulus. Transient IOSs were highly correlated with ON and OFF edges of the light stimulus. Fast IOSs occurred rapidly (<10 ms) after the stimulus onset. Most of the fast IOSs could reach the maximum magnitude (black arrowheads in Fig. 2(d)) within 100 ms after the stimulus onset. An additional change of responses was typically observed within 1 s after the stimulus offset (gray arrowheads in Fig. 2(d)).

3.2. *Positive and negative IOSs with different time courses*

From Fig. 2, we observed that IOSs at adjacent retinal locations could be both positive and negative going. The IOSs of individual pixels (tracings 1–6 in Fig. 2(d)) could often exceed 10% $\Delta I/I$. However, when signals of an extended retinal area were averaged (tracing 7 in Fig. 2(d)), the response was at least one order of magnitude smaller, due to the cancellation of positive and negative signals. Figure 3 shows the spatiotemporal distribution of the IOSs with opposite polarities. After the stimulus onset, early positive and negative optical response (such as the third frames of Figs. 3(a) and 3(b)) had similar spatial distribution. After the stimulus offset, however, the positive signal pattern shrunk gradually (Fig. 3(a)), while the negative signal pattern expanded over time (Fig. 3(b)). The expanding process of the negative pattern could last at least six seconds. Overall, the early optical response was dominated by positive optical signals; while the

later optical response was dominated by negative signals (Fig. 3(c)).

3.3. *Dynamic differential IOS imaging*

Figure 4 shows differential IOS images recorded from the same frog eye used for the experiment shown in Figs. 2 and 3. Given the fact that the dynamic differential processing acted as a high-pass filter, the slow component of the IOSs shown in Figs. 2 and 3 was reduced; while fast optical responses associated with ON and OFF edges of the visible light stimulus were enhanced. Figure 4(b) shows the statistics of activated retinal area. A threshold ($|IOS| > 2.5\%\ \Delta I/I$) was used to reduce the effect of background noises on the statistics. From Fig. 4, we observed that transient IOSs occurred immediately after stimulus onset, and fractional value of activated retinal area could reach a magnitude peak within 50 ms (black arrowhead in Fig. 4(b)) after the stimulus onset. An additional peak (gray arrowhead in Fig. 4(b)) was observed within 0.5 s after the stimulus offset.

4. Discussion

In summary, we demonstrated that NIR light imaging of fast IOSs could be obtained from isolated frog eye through intact ocular optics. Fast IOSs had time courses that were tightly correlated with the ON and OFF edges of the stimulus, and thus might reflect dynamic neural activities of activated retinal neurons directly. Slow IOSs (e.g. recovery phase of the tracing 7 in Fig. 2(d)) could last a relatively long time (>6 s), and did not return to pre-stimulus baseline within the recording time. Dynamic differential IOS imaging (Fig. 4) can provide a simple strategy to minimize the effect of slow optical responses on fast IOSs, which are most interesting for direct evaluation of fast retinal neural activity. While major part of the slow IOSs may result from stimulus-associated metabolic changes of the retina and other ocular tissues, dynamic phototransduction procedures of photoreceptors may also partially contribute to transient IOSs. Previous studies with isolated photoreceptor outer segments and isolated retinas have demonstrated transient IOSs associated with phototransduction.[31–33] Both binding and release of G-proteins to photoexcited rhodopsin may contribute to transient IOSs.[33] While on-going phase of the phototransduction-associated optical changes occurred immediately after the stimulus, the recovery phase could last for a relatively long time.[33]

Transient IOSs with both positive and negative polarities were observed at adjacent retinal locations. Different dynamics, in term of time course and optical patterns (Fig. 3), of transient IOSs with opposite polarities suggest multiple sources, or mechanisms, of the IOSs. We hypothesize that positive IOSs result primarily from scattering changes due to transient mechanical (swelling or shrinking) dynamics of stimulus activated retinal neurons[34,35]; while negative IOSs, particularly slow negative IOSs in the edge of the stimulus activated retinal area (Fig. 3(b)), may mainly relate to absorption changes correlated with stimulus activated metabolic procedures of the retina and other ocular tissues. Further study is required for better understanding of the sources and mechanisms of positive and negative IOSs with different time courses.

Our experimental results indicated that high spatial resolution was required to differentiate positive and negative IOSs in adjacent retinal areas. Dynamic optical change at individual CCD pixels could often exceed 10% of the background light intensity (Fig. 2). Recording at a low spatial resolution could pool responses of opposite polarity together, and thus reduce recorded signal magnitude or even fail to record fast IOSs (Fig. 2). We anticipate that further development of fast (>100 Hz), high(sub-cellular)-resolution fundus imager, with sophisticated data processing system, will allow robust detection of fast IOSs *in vivo*, and thus allow noninvasive, three-dimensional evaluation of retinal neural function. High-resolution imaging of retinal neural function will provide improved retinal diagnosis and treatment evaluation.

Acknowledgments

This research was supported by Eyesight Foundation of Alabama and Dana Foundation (Brain and Immuno-Imaging Grant Program).

References

1. Hogg, R. E. and Chakravarthy, U., "Visual function and dysfunction in early and late age-related maculopathy," *Prog. Retin. Eye Res.* **25**, 249–276 (2006).
2. Harwerth, R. S. and Quigley, H. A., "Visual field defects and retinal ganglion cell losses in patients

with glaucoma," *Arch. Ophthalmol.* **124**, 853–859 (2006).
3. Nickells, R. W., "Ganglion cell death in glaucoma: From mice to men," *Vet. Ophthalmol.* **10 Suppl 1**, 88–94 (2007).
4. Meyer-Rusenberg, B., Pavlidis, M., Stupp, T. and Thanos, S., "Pathological changes in human retinal ganglion cells associated with diabetic and hypertensive retinopathy," *Graef. Arch. Clin. Exp.* **245**, 1009–1018 (2007).
5. Qin, Y. W., Xu, G. Z. and Wang, W. J., "Dendritic abnormalities in retinal ganglion cells of three-month diabetic rats," *Curr. Eye Res.* **31**, 967–974 (2006).
6. Kolb, H., Fernandez, E. and Nelson, R., "Gross Anatomy of the Eye," http://webvision.med.utah.edu/anatomy.html. (2003).
7. Falsini, B., Marangoni, D., Salgarello, T., Stifano, G., Montrone, L., Campagna, F., Aliberti, S., Balestrazzi, E. and Colotto, A., "Structure-function relationship in ocular hypertension and glaucoma: Interindividual and interocular analysis by OCT and pattern ERG," *Graefes. Arch. Clin. Exp. Ophthalmol.* **246**, 1153–1162 (2008).
8. Oishi, A., Otani, A., Sasahara, M., Kurimoto, M., Nakamura, H., Kojima, H. and Yoshimura, N., "Retinal nerve fiber layer thickness in patients with retinitis pigmentosa," *Eye* (2008).
9. Scholl, H. P. and Zrenner, E., "Electrophysiology in the investigation of acquired retinal disorders," *Survey of Ophthalmology* **45**, 29–47 (2000).
10. Hood, D. C., "Assessing retinal function with the multifocal technique," *Prog. Retin. Eye Res.* **19**, 607–646 (2000).
11. Hood, D. C., Odel, J. G., Chen, C. S. and Winn, B. J., "The multifocal electroretinogram," *J. Neuroophthalmol.* **23**, 225–235 (2003).
12. Rector, D. M., Carter, K. M., Volegov, P. L. and George, J. S., "Spatio-temporal mapping of rat whisker barrels with fast scattered light signals," *Neuroimage* **26**, 619–627 (2005).
13. Chance, B., Luo, Q., Nioka, S., Alsop, D. C. and Detre, J. A., "Optical investigations of physiology: A study of intrinsic and extrinsic biomedical contrast," *Philos. Trans. R. Soc. Lond. B Biol. Sci.* **352**, 707–716 (1997).
14. Chen, S., Li, P., Luo, W., Gong, H., Zeng, S. and Luo, Q., "Time-varying spreading depression waves in rat cortex revealed by optical intrinsic signal imaging," *Neurosci. Lett.* **396**, 132–136 (2006).
15. Grinvald, A., Lieke, E., Frostig, R. D., Gilbert, C. D. and Wiesel, T. N., "Functional architecture of cortex revealed by optical imaging of intrinsic signals," *Nature* **324**, 361–364 (1986).
16. Hoshi, Y., Oda, I., Wada, Y., Ito, Y., Yutaka, Y., Oda, M., Ohta, K., Yamada, Y. and Mamoru, T., "Visuospatial imagery is a fruitful strategy for the digit span backward task: A study with near-infrared optical tomography," *Brain Res. Cogn. Brain Res.* **9**, 339–342 (2000).
17. Yao, X. C. and George, J. S., "Dynamic neuroimaging of retinal light responses using fast intrinsic optical signals," *Neuroimage* **33**, 898–906 (2006).
18. Abramoff, M. D., Kwon, Y. H., Ts'o, D., Soliz, P., Zimmerman, B., Pokorny, J. and Kardon, R., "Visual stimulus-induced changes in human near-infrared fundus reflectance," *Invest. Ophthalmol. Vis. Sci.* **47**, 715–721 (2006).
19. Hanazono, G., Tsunoda, K., Shinoda, K., Tsubota, K., Miyake, Y. and Tanifuji, M., "Intrinsic signal imaging in macaque retina reveals different types of flash-induced light reflectance changes of different origins," *Invest. Ophthalmol. Vis. Sci.* **48**, 2903–2912 (2007).
20. Nelson, D. A., Krupsky, S., Pollack, A., Aloni, E., Belkin, M., Vanzetta, I., Rosner, M. and Grinvald, A., "Special report: Noninvasive multi-parameter functional optical imaging of the eye," *Ophthalmic Surg. Lasers Imaging* **36**, 57–66 (2005).
21. Grieve, K. and Roorda, A., "Intrinsic signals from human cone photoreceptors," *Invest. Ophthalmol. Vis. Sci.* **49**, 713–719 (2008).
22. Jonnal, R. S., Rha, J., Zhang, Y., Cense, B., Gao, W. H. and Miller, D. T., "*In vivo* functional imaging of human cone photoreceptors," *Optics Express* **15**, 16141–16160 (2007).
23. Yao, X. C., Yamauchi, A., Perry, B. and George, J. S., "Rapid optical coherence tomography and recording functional scattering changes from activated frog retina," *Applied Optics* **44**, 2019–2023 (2005).
24. Srinivasan, V. J., Wojtkowski, M., Fujimoto, J. G. and Duker, J. S., "*In vivo* measurement of retinal physiology with high-speed ultrahigh-resolution optical coherence tomography," *Opt. Lett.* **31**, 2308–2310 (2006).
25. Bizheva, K., Pflug, R., Hermann, B., Povazay, B., Sattmann, H., Qiu, P., Anger, E., Reitsamer, H., Popov, S., Taylor, J. R., Unterhuber, A., Ahnelt, P. and Drexler, W., "Optophysiology: Depth-resolved probing of retinal physiology with functional ultrahigh-resolution optical coherence tomography," *Proc. Nat. Acad. Sci. USA* **103**, 5066–5071 (2006).
26. Zhao, Y. B. and Yao, X. C., "Intrinsic optical imaging of stimulus-modulated physiological responses in amphibian retina," *Opt. Lett.* **33**, 342–344 (2008).
27. Yao, X. C. and Zhao, Y. B., "Optical dissection of stimulus-evoked retinal activation," *Opt. Express* **16**, 12446–12459 (2008).

28. Yao, X. C. and George, J. S., "Near-infrared imaging of fast intrinsic optical responses in visible light-activated amphibian retina," *J. Biomed. Opt.* **11**, 064030 (2006).
29. Meister, M., Pine, J. and Baylor, D. A., "Multi-neuronal signals from the retina: Acquisition and analysis," *J. Neurosci. Methods* **51**, 95–106 (1994).
30. Aho, A. C., "The visual acuity of the frog (*Rana pipiens*)," *J. Comp. Physiol. [A]* **180**, 19–24 (1997).
31. Arshavsky, V. Y., Lamb, T. D. and Pugh, Jr., E. N., "G-proteins and phototransduction," *Ann. Rev. Physiol.* **64**, 153–187 (2002).
32. Hofmann, K. P., Uhl, R., Hoffmann, W. and Kreutz, W., "Measurements on fast light-induced light-scattering and -absorption changes in outer segments of vertebrate light sensitive rod cells," *Biophys. Struct. Mech.* **2**, 61–77 (1976).
33. Kuhn, H., Bennett, N., Michel-Villaz, M. and Chabre, M., "Interactions between photoexcited rhodopsin and GTP-binding protein: Kinetic and stoichiometric analyses from light-scattering changes," *Proc. Nat. Acad. Sci. USA* **78**, 6873–6877 (1981).
34. Yao, X. C., Rector, D. M. and George, J. S., "Optical lever recording of displacements from activated lobster nerve bundles and Nitella internodes," *Appl. Opt.* **42**, 2972–2978 (2003).
35. Yao, X. C., Foust, A., Rector, D. M., Barrowes, B. and George, J. S., "Cross-polarized reflected light measurement of fast optical responses associated with neural activation," *Biophys. J.* **88**, 4170–4177 (2005).